J Mater Sci: Mater Med (2011) 22:217–227
DOI 10.1007/s10856-010-4203-5

Synthesis, bioactivity and preliminary biocompatibility studies of glasses in the system $CaO–MgO–SiO_2–Na_2O–P_2O_5–CaF_2$

D. U. Tulyaganov · S. Agathopoulos · P. Valerio · A. Balamurugan · A. Saranti · M. A. Karakassides · J. M. F. Ferreira

Received: 26 February 2009 / Accepted: 30 November 2010 / Published online: 29 December 2010

Abstract New compositions of bioactive glasses are proposed in the $CaO–MgO–SiO_2–Na_2O–P_2O_5–CaF_2$ system. Mineralization tests with immersion of the investigated glasses in simulated body fluid (SBF) at 37°C showed that the glasses favour the surface formation of hydroxyapatite (HA) from the early stages of the experiments. In the case of daily renewable SBF, monetite ($CaHPO_4$) formation competed with the formation of HA. The influence of structural features of the glasses on their mineralization (bioactivity) performance is discussed. Preliminary in vitro experiments with osteoblasts' cell-cultures showed that the glasses are biocompatible and there is no evidence of toxicity. Sintering and devitrification studies of glass powder compacts were also performed. Glass-ceramics with attractive properties were obtained after heat treatment of the glasses at relatively low temperatures (up to 850°C).

1 Introduction

Since the discovery of Bioglass® by Hench [1], bioactive glasses have been intensively studied due to their biocompatibility and ability for developing strong bonding to bones, attributed to a carbonated partially-substituted hydroxyapatite (HCA) layer growing on their surface, similar to mineral part of bones [2–9]. In the body, HCA forms via a sequence of reactions occurring between the surface of implanted bioactive glasses and the surrounding tissues or biological liquids [10]. The widely accepted mechanism of hydroxyapatite (HA) formation on silicate bioactive glasses [11–17], experimentally verified both in vitro and in vivo [18–20]. This mechanism involves dissolution of Ca^{2+} ions from the surface of bioactive glasses that increases the supersaturation in the surrounding liquid, with respect to HA components, and enables precipitation of HA on the surface of glasses, which has been already transformed (due to leaching effect) into a layer with features of silica-gel.

With regards to compositions, a wide bioactive composition region is known in the $Na_2O–CaO–SiO_2$ ternary system [5]. This region overlaps the bioactivity region of the P_2O_5-containing $Na_2O–CaO–SiO_2$ system, being, however, somewhat curtailed in the SiO_2-poor region, but more extended towards the $Na_2O–SiO_2$ and the $CaO–SiO_2$ regions. The kinetics of HA formation seemingly depends on Na_2O/CaO ratio. Little differences in apatite formation rates have been reported between the P_2O_5-containing Bioglass® 45S5 and the corresponding P_2O_5-free $Na_2O–CaO–SiO_2$ glass. The study of different compositions in the ternary $Na_2O–SiO_2–CaO$ system with 6 wt% P_2O_5 showed that 45S5 Bioglass® (45 SiO_2, 24.5 Na_2O, 24.5 CaO, 6 P_2O_5, in wt%) exhibited the highest bioactivity. Nowadays, 45S5 Bioglass® is used as middle ear and dental implants [21].

However, there are specific bone restoration and regeneration needs, including scaffolds for bone tissue engineering, which require controllable bioactivity and gradual resorption of implants (i.e. not very intensive or

D. U. Tulyaganov · A. Balamurugan · J. M. F. Ferreira (✉)
Department of Ceramics and Glass Engineering, University of Aveiro, CICECO, 3810-193 Aveiro, Portugal
e-mail: jmf@ua.pt

S. Agathopoulos · A. Saranti · M. A. Karakassides
Department of Materials Science and Engineering, University of Ioannina, Greece, 451 10 Ioannina, Greece

P. Valerio
Department of Biophysics and Physiology, Federal University of Minas Gerais, ICB-UFMG, Belo Horizonte, MG 31270-901, Brazil

very fast, respectively) to enable concurrent replacement by newly formed bone [22, 23]. In this aspect, it must be also mentioned that degradation products of bioactive glasses can suitably activate gene expression of osteoblasts, stimulate production of growth factors, and favour cell proliferation [24].

In this regard, in our earlier study [25], we have shown that glasses in the CaO–MgO–SiO_2 system with additives of B_2O_3, P_2O_5 and Na_2O possess in vitro bioactivity features. Dissolution phenomena and formation of microcrystallites account for structural modifications taking place at the surface of the glasses from the very beginning of immersion in simulated body fluid (SBF, [26]) at 37°C. There was evidence of formation of both silica-gel and HA at the surface of those glasses. Glass surfaces were completely covered with HA layer after 2–3 weeks in SBF. The influence of the structural features of those glasses on bioactivity performance was evident after prolong immersion (120 days) in SBF. It was demonstrated that increasing amount of phosphates (up to 6.32 wt% P_2O_5) favours deposition of A-type carbonated HA.

In this paper, we present two brand-new compositions of bioactive glasses, whose compositions are shown in Table 1. According to Table 1, the new compositions derive from composition G-1b, thoroughly studied in our earlier study [25], but they are B-free G-1b precisely corresponds to the composition 1b reported in [25]; here, G stands for glass. With respect to the molecular formula of glass G-1b ($Na_2O{\cdot}B_2O_3{\cdot}3MgO{\cdot}7CaO{\cdot}9SiO_2{\cdot}0.60P_2O_5{\cdot}CaF_2$), B_2O_3–substitution takes place in the first new glass (designated for simplicity reasons as G-1d) according to the scheme $2B^{3+} \rightarrow 1.5Si^{4+}$, and in the second glass (designated as G-1e) $2B^{3+} \rightarrow Si^{4+} + 0.2P^{5+} + 0.5Ca^{2+}$. Accordingly, glass G-1d is slightly richer in Si^{4+} and poorer in Ca^{2+} and P^{5+} than glass G-1e.

The bioactivity and biocompatibility of the new compositions was assessed through immersion tests in simulated body fluid (SBF) and in vitro osteoblasts' cells-cultures, respectively, to evaluate their potential for further consideration and experimentation in biomedical applications. The relationship between the properties and the structure of the glasses is highlighted. The devitrification behaviour of the glasses after heat treatment at temperatures up to 850°C was also investigated.

2 Materials and experimental procedure

2.1 Preparation of glasses and crystallization experiments

Powders of technical grade of silicon oxide (purity >99.5%) and calcium carbonate (>99.5%) and of reagent grade of $4MgCO_3{\cdot}Mg(OH)_2{\cdot}5H_2O$, Na_2CO_3, CaF_2, and $NH_4H_2PO_4$ were used. Homogeneous mixtures of batches ($\sim$100 g) of the compositions reported in Table 1, obtained by ball-milling, were preheated at 1000°C for 1 h for decarbonization and then completely melted in Pt-crucibles at 1400°C for 1 h, in air. Both bulk (i.e. in block form) samples and glass frit were produced.

Blocks of bulk transparent and colourless glasses were produced by casting the melts on preheated bronze moulds, with subsequent immediate annealing at 600°C (i.e. close to glass transition points T_g) for 1 h. The surfaces of the bulk samples were mirror polished (i.e. final polishing with 1 μm diamond paste) and then cleaned by ultrasonic agitation.

Glass-frits were obtained by quenching of the melts into cold water. The frits were dried and then milled in a high-speed porcelain mill (Nannetti, Faenza, Italy; balls/material weight ratio was approximately 1.5) and passed through an

Table 1 Chemical compositions (batches) of the investigated glasses G-1d and G-1e (the composition of glass G-1b [25] is presented for comparison purposes)

Glass	SiO_2	B_2O_3	CaO	MgO	P_2O_5	Na_2O	CaF_2
G-1b [25]							
wt%	40.08	5.16	29.10	8.96	6.32	4.59	5.79
mol%	39.82	4.43	30.97	13.27	2.65	4.43	4.43
mol ratio	9	1	7	3	0.60	1	1
G-1d							
wt%	46.06	–	28.66	8.83	6.22	4.53	5.70
mol%	45.45	–	30.30	12.99	2.60	4.33	4.33
mol ratio	10.5	–	7	3	0.60	1	1
G-1e							
wt%	43.48	–	30.44	8.75	7.19	4.49	5.65
mol%	43.10	–	32.33	12.93	3.02	4.31	4.31
mol ratio	10	–	7.5	3	0.70	1	1

80 μm sieve to obtain fine powders with 11–14 μm mean particle size (determined by light scattering technique, Coulter LS 230, UK, Fraunhofer optical model) and 0.3–0.7 m^2/g specific surface area (measured by BET technique, Micromeritics, Gemini II 2370, USA).

Annealed bulk glass blocks were used for dilatometry measurements (Bahr Thermo Analyse DIL 801 L, Germany, heating rate 5 K/min; cross section of samples 4×5 mm^2; for comparison purposes, similar block samples of the previously produced glass G-1b [25] were also measured under the same conditions).

According to our experience on a similar system [25], crystallization experiments were preferably carried out with glass powder-compacts (than bulk glass blocks). Powder of glass frit was granulated (by stirring in a mortar) in a 5 vol.% polyvinyl alcohol solution (PVA, Merck; the solution of PVA was made by dissolution in warm water) in a proportion of 97.5 wt% of frit and 2.5 wt% of PVA. Rectangular bars ($4 \times 5 \times 50$ mm^3) were prepared by uniaxial pressing (80 MPa) of the granulated glass powders into a special mould. The bars were sintered at different temperatures up to 850°C for 1 h in air with slow heating and cooling rates of 2 K/min. The crystallized phases of sintered glass powder-compacts were identified by X-ray diffraction (XRD, Rigaku Geigerflex D/Mac, C Series, Cu K_a radiation, Japan). Copper K_α radiation ($\lambda = 1.5406$ Å), produced at 30 kV and 25 mA, scanned the range of diffraction angles (2θ) between 10° and 60° with a 2θ-step of 0.02°/s. The phases were identified by comparing the experimental X-ray patterns to standards complied by the International Centre for Diffraction Data (ICDD).

2.2 Mineralization tests in SBF

The in vitro bioactivity of glasses, reflected in their capability of inducing HA-formation onto their surfaces, was investigated by immersion of either block samples or fine glass powders in SBF at 37 ± 0.1°C. SBF had an ionic concentration (in mM) of 142.0 Na^+, 5.0 K^+, 2.5 Ca^{2+}, 1.5 Mg^{2+}, 147.8 Cl^-, 4.2 HCO_3^-, 1.0 HPO_4^{2-} and 0.5 SO_4^{2-}, buffered at pH 7.25 with tris-hydroxymethyl-aminomethane (Tris, 50 mM) and hydrochloric acid solutions [26]. The SBF was filtered through sterilized filters (cameo 25 AS-MSI, pore size 0.22 μm). Sterilized glass flasks were used for the experiments.

In this study, we carried out both "static SBF" and "semi-dynamic SBF" tests, where the latter means that we renewed the liquid with fresh SBF every day. In the case of powders, we exposed ~1 m^2 in 10 ml SBF. Each sample was individually tested so that the results could be obtained without interfering with other samples.

Raman spectroscopy (micro Raman system, Renishaw 1000, UK), using the 532 nm line of a solid state laser at 60 mW for excitation, was employed to investigate the structural modifications of the surface of bulk samples over immersion time in SBF. Raman spectra were collected by means of a microscope (Leica, UK) equipped with lenses 50× and 100×. Infrared spectra of glass powders, consolidated into pellets with the aid of KBr powder, were measured with a Fourier transform spectrometer (Perkin Elmer Spectrum GX) in the frequency range of 400–2000 cm^{-1}. The presenting spectra are the average of 25 scans recorded at 2 cm^{-1} resolution.

Microstructure observations of surfaces of bulk samples were done with a field emission scanning electron microscope (FE-SEM Hitachi S-4100, Japan; 25 kV acceleration voltage, beam current 10 μA) under secondary electron mode, equipped with energy dispersive spectroscope (EDS) for chemical analysis. The crystalline phases developed in the powders were identified with XRD analysis (in the range 20°–50°).

2.3 In vitro tests with cell-cultures of osteoblasts

The preliminary in vitro tests with osteoblasts were carried out according to the methodology described in [24]. The following materials were used: RPMI (Gibco BRL. NY, USA) medium supplemented with 10% FBS and 1% antibiotic–antimycotic (Sigma, St. Louis, USA); Dulbecco's phosphate buffered saline, trypsin–EDTA, [3(4,5dimethylthiazol-2yl)2,5diphenyltetrazoliumbromide] MTT, BCIP-NBT (Gibco, Burlington, Ontario, Canada); Crude bacterial collagenase (Boehringer, Biberach, Germany); SIRCOL kit (Biocolor, Newtonabbey, Northern Ireland); T25 culture flasks and 24 well plates (Nunc products, Naperville, USA).

Osteoblasts were isolated from the calvaria of 1–5 days old neonatal Wistar rats [27]. The calvaria were dissected and freed from soft tissue, cut into small pieces and rinsed in phosphate-buffered saline without calcium and magnesium. The calvaria pieces were incubated with 1% trypsin–EDTA for 5 min, followed by four sequential digestions (30 min each) with 0.02% collagenase at 37°C for 45 min each. The supernatant of the first collagenase digestion, which contains a high proportion of periosteal fibroblasts, was discarded. The other digestions produced a suspension of cells with high proportion of osteoblasts. After centrifugation at 1000 g for 5 min, each pellet was re-suspended in 5 ml of culture medium. The cells were seeded into 25 ml tissue culture flasks and led to grow in a controlled 5% CO_2, 95% humidified incubator at 37°C.

Osteoblasts were platted in a 1×10^5 cell density, at passage 2, in 24 well plates. After 2 h, the medium was changed to a medium containing the fine glass powders at a concentration of 0.005 g glass powder/1 ml culture medium. After 72 h of incubation, osteoblasts' morphology, viability/proliferation and secretion capability were tested.

After 72 h of incubation in the presence of each of the tested powders, osteoblasts' viability was evaluated by the MTT assay, based on the reduction of tetrazolium salt to formazan crystals by dehydrogenase present in living cell mitochondria. The formazan salt formation is directly related to the amount of dehydrogenase, providing an indirect measurement of cell viability [28]. 60 µl of MTT (5 mg/ml) were added to each well. 2 h later, the cell morphology was analyzed by inverted optical microscopy and formazan salts were solubilised with 100 µl SDS 10% HCl. After incubation for 18 h, optical density was measured at 595 nm [29].

The osteoblasts collagen production was measured in the cultures supernatant by SIRCOL assay [30]. The method is based on the selective binding property of the syrius-red dye to the [Gly–X–Y] tripeptide end sequence of mammalian collagen. The syrius-red/collagen precipitate can be solubilised and the optical density was measured at 595 nm. The alkaline phosphatase production was evaluated by the BCIP-NBT assay. This assay is based on a chromagenic reaction initiated by the cleavage of the phosphate group of BCIP by alkaline phosphatase present in the cells. This reaction produces a proton which reduces NBT to an insoluble purple precipitate. In brief, the supernatant of each well was removed and the cell layer was rinsed twice with PBS. Then, 200 µl of BCIP-NBT solution, prepared according to the manufacturer protocol, were added to each well. After 2 h of incubation, the cells were observed by optical microscopy and the insoluble purple precipitates were solubilised with 210 µl of SDS 10% HCl and incubated for 18 h. The optical density was measured at 595 nm [31].

The results are presented as means ± SD. The statistical significance was measured by ANOVA and Bonferroni's post-test (confidence level was 95%; controls were osteoblasts incubated in the same conditions but in the absence of glass particles).

3 Results

The two investigated glasses could be completely melted after 1 h at 1400°C and easily cast, resulting in transparent and colourless blocks with no crystalline inclusions as confirmed by X-ray and SEM analyses.

The dilatation curves of the glasses are plotted in Fig. 1 (the curve of the parent glass G-1b is also plotted for comparison purposes) and their analysis, with regards to the transition (T_g) and softening points (T_s) as well as the coefficients of thermal expansion (CTE) determined from the slope of the linear part of the curves, is summarized in Table 2. Accordingly, T_g ranged between 580 and 600°C, T_s between 644 and 672°C, while the CTE values were

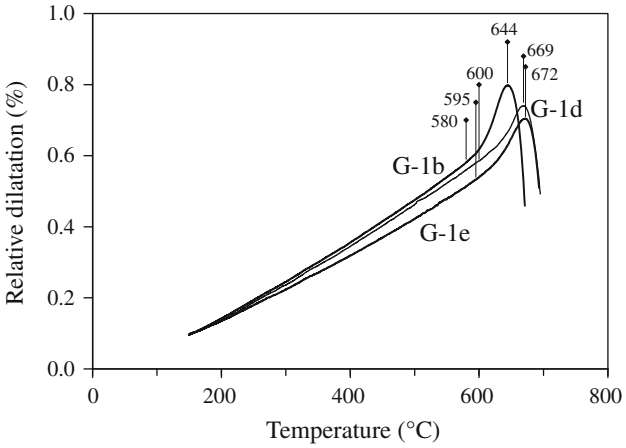

Fig. 1 Dilatometry curves of the as-cast and annealed bulk glasses

Table 2 Characteristic temperatures (T_g and T_s) of the glasses G-1b, G-1d and G-1e and their thermal expansion coefficients (CTE) for the temperature ranges of 200–400°C and 200–500°C determined from the dilatometry curves of Fig. 1

	G-1b	G-1d	G-1e
T_g (°C)	580	600	595
T_s (°C)	644	669	672
CTE ($\times 10^{-6}$ K^{-1})			
200–400°C	10.67	10.44	9.18
200–500°C	11.11	10.87	9.56

generally high in the level of $\sim 10 \times 10^{-6}$ K^{-1} but the CTE of glass G-1e is slightly less than G-1d.

Heat treatment of the glass powder compacts at 700°C (i.e. above T_g) showed that the samples maintained their amorphous nature but were completely dense indicating that sintering precedes crystallization in these systems. Devitrification occurred after heat treatment at higher temperatures. Figure 2 shows the X-ray diffractograms of the tested glasses after heat treatment at 800°C. Pyroxene phase diopside predominantly formed. There was evidence of formation of wollastonite and fluorapatite as well. The same assemblage of phases, but with a significant increase in intensity, was registered in the diffractograms of samples heat treated at 850°C. Dense glass-ceramic samples of white colour and attractive appearance with no-cracks or visible open porosity were obtained after heat treatment at both 800 and 850°C.

Surface modifications occurred after immersion of either block or fine powder glass samples in SBF. The structural surface modifications occurred in the bulk samples of the glasses G-1d and G-1e in static-SBF experiments are reflected in the Raman spectra of Fig. 3. The spectra of intact glasses exhibit a dominant band at about 960 cm^{-1} with two broad shoulders at ca. 1050 and 880 cm^{-1}, a band

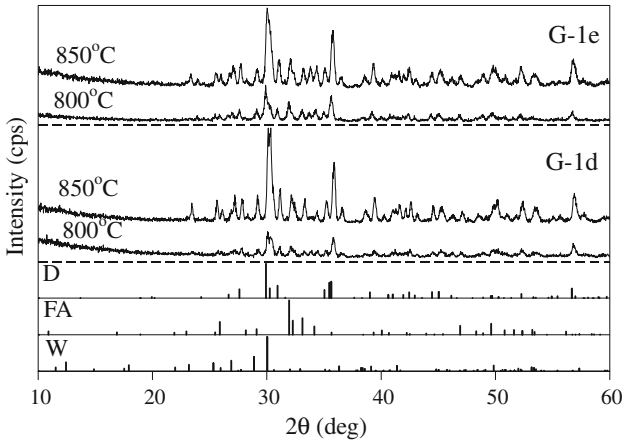

Fig. 2 X-ray diffractograms of the glass-powder compacts heat treated at 800 and 850°C for 1 h in air. (Diopside (D), $CaMgSi_2O_6$, ICDD card: 01-071-1067; Fluorapatite (FA), $Ca_5(PO_4)_3F$, ICDD card: 01-071-0880; Wollastonite (W), $CaSiO_3$, ICDD card: 00-042-0550; the diffractograms have not been normalized; full-scale of intensity axis: 5.000 cps)

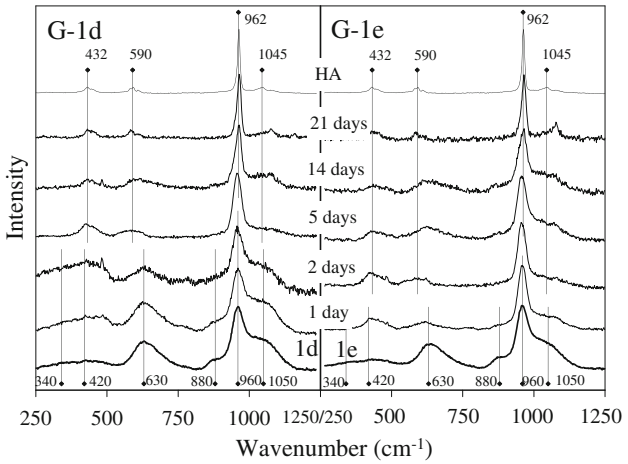

Fig. 3 Evolution of Raman spectra obtained from the surface of bulk glass samples over immersion time in SBF ("static" experiments) at 37°C. The spectrum of HA is also plotted for comparison purposes. (For facilitating comparison, the spectra have been normalized)

at 630 cm^{-1} and a broad band envelope doubly peaking at 340 and 420 cm^{-1}. The general assignments of these bands are summarized in Table 3.

After 1 and 2 days of immersion in SBF, the spectra of glass G-1d seem to retain the main features of the intact glass since the bandwidth of the main band at 960 cm^{-1} remains unchanged and the bands due to the phosphate glass network at 1050 and 630 cm^{-1} are still clearly observable. Significant changes seem to have occurred at the surface of glass G-1e after only 1 day in SBF. The bandwidth of the band at 960 cm^{-1} decreases from $\sim 50^{-1}$ to ~ 35 cm^{-1} and the bands due to phosphate units of the glass network (630, 880, 1050 cm^{-1}) diminish.

The surfaces of both glasses undergo modifications that lead to well-developed HA after 21 days (the typical Raman spectrum of HA, also plotted at the top of Fig. 3 for comparison purposes, exhibits a strong peak at 962 cm^{-1} and three weaker bands peaking at 1045, 590, and 432 cm^{-1} [32]). Observations of the surfaces of the samples with optical microscope and SEM (not shown) agreed fairly well to the Raman spectra evolution of Fig. 3, because they confirmed a regular development of (the EDS spectrum registered Ca and P peaks with a Ca/P ratio of ~ 1.67). The calcium phosphate layer completely covered the surface of glass samples after 3 weeks in SBF.

In the case of the semi-dynamic SBF tests (where SBF was daily renewed), the results of X-ray diffraction (Fig. 4) of fine powders show that monetite ($CaHPO_4$) competes (and can form together with) HA. Formation of monetite is seemingly favoured in short immersion times and more in the glass G-1e than in the glass G-1d. The SEM images of Fig. 5 (pay attention to the scale bars), which show the surfaces of bulk glasses after immersion in SBF in semi-dynamic conditions, agree fairly well with the diffractograms of Fig. 4. In Fig. 5a, big Ca/P-containing precipitates (according to EDS), apparently of amorphous nature, are observed on the surface of glass G-1d just after 1 day of immersion. However, it is not clear if they are well adjoined to glass surface or not. Extensive corrosion

Table 3 General assignments of Raman (Fig. 3) and IR bands (Fig. 6) to structural features of the (intact) glasses G-1d and G-1e [25]

Band (cm^{-1})		Assignment
Raman	IR	
1100	1075	Q^3 units ($Si\emptyset_3O^-$)
950	950	Q^2 units ($Si\emptyset_2O_2^{2-}$)
900	900	Q^1 units ($Si\emptyset O_3^{3-}$)
850		Q^0 units (SiO_4^{4-})
550–750	400–550, 780	Si–O–Si (Q^2 units at 650 cm^{-1}, Q^1 units high frequency asymmetry at 650 cm^{-1})
1020–1050		Si–O^0 from Q^3, Q^2 and Q^1 units or vibrations in structural units associated with alkali metal cations
950–980, 590, 425	1400–400	P–O^- bonds and O–P–O bridges in PO_4^{3-} units

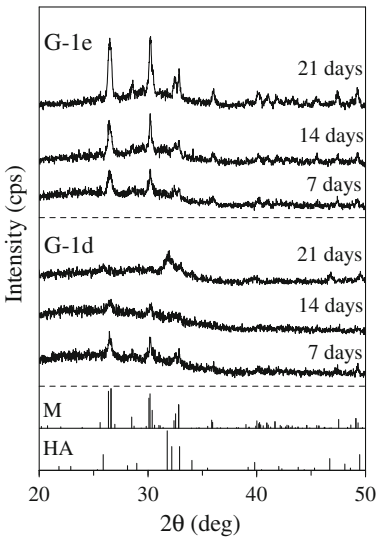

Fig. 4 X-ray diffractograms of the powders of the investigated glasses after immersion in renewable SBF ("semi-dynamic" experiments) at 37°C for different times. (HA, ICDD card: 00-009-0432; Monetite (M), $CaHPO_4$, ICDD card: 01-089-5969; the diffractograms have not been normalized; full-scale of intensity axis: 5.500 cps)

of glass surface is also evident. Figure 5b, c and d shows the morphology of a network of HA (at three different magnifications) developed on the surface of glass G-1d after 3 weeks in SBF. On the surface of glass G-1e we observed big prismatic (with triangular aspect) well-developed crystals after 3 weeks in SBF (Fig. 5e and f). With respect to HA stoichiometry, EDS chemical analysis showed that they were Ca-deficient (i.e. Ca/P $\approx 1 < 1.67$ of HA). Hence, in conjunction with the result of XRD analysis (Fig. 4), the crystals of Fig. 5e and f, which also greatly resemble the morphology of monetite crystals presented in [33], should be attributed to monetite.

The formation of monetite and its competition with HA is also suggested in the IR spectra of glass powders immersed in SBF under semi-dynamic conditions for different times (Fig. 6). The IR-spectra of the intact glasses exhibit a strong absorption band envelope in the frequency region of 800–1200 cm^{-1} with two maxima at 1030 and 950 cm^{-1}, a shoulder at 870 cm^{-1} and a band at 500 cm^{-1}. The general assignments of these bands are summarized in Table 3.

In the glass G-1d, the modifications occurred after 7 days in SBF resulted in developing of new bands at 1133, 1070, and 998 cm^{-1}, attributed to P–O stretching vibrations of monetite ($CaHPO_4$) [34]. However, the spectrum of glass G-1d after 21 days in SBF shows characteristic bands of HA (also plotted at the top in the diagram of Fig. 6, for comparison purposes). The spectrum of glass G-1e shows also the development of new bands due to the vibrations of structural units of monetite after 3 days in SBF. These bands become sharper over immersion time but there is not evidence of HA formation after 3 weeks in SBF.

As far as the in vitro biocompatibility tests are concerned, the osteoblasts remained viable and continued to proliferate after 3 days in culture in the presence of the investigated glasses. The powder of glass G-1d induced significant increase of proliferation when compared to control and glass G-1e that was also higher than control (Fig. 7a). Osteoblasts collagen secretion was not altered when the cells were incubated in the presence of the glass powders (Fig. 7b), while alkaline phosphatase production decreased comparing to control (Fig. 7c).

4 Discussion

4.1 Mineralization capability

The classic SBF-immersion tests (i.e. static-SBF) showed that the investigated new glasses G-1d and G-1e are bioactive because HA well develops on their surfaces after 3 weeks. The transformation of glass surface structure (and chemistry), leading to HA-formation, occurs from the early stages of mineralization (Fig. 3). There was no evidence of monetite formation in the static-SBF experiments (Fig. 3 and Raman spectra of monetite of ref. [34]).

The tests performed under semi-dynamic SBF conditions resulted in a competition between monetite and HA formation (Figs. 4, 5, 6). It is known HA layer forms faster in static systems than in slow flowing and circulating systems [35], but in vitro tests carried out in dynamic flow of SBF simulate better the in vivo conditions, making the latter tests more precise and reliable [36]. Monetite ($CaHPO_4$) is a Ca-deficient (with respect to HA) compound. Hence, it is suggested that the daily renewing of SBF ceases Ca^{2+} supersaturation (with respect to HA) in the solution [37] and/or locally at the surface of the glass, favouring the monetite formation [36]. Monetite is a precursor of HA since it serves as a substrate for the oriented re-precipitation of HA crystallites [33], and its bioactivity has been well-documented [38].

Beyond the above general conclusions, valid for both investigated glasses, the experimental results revealed small differences in bioactivity performance between the glasses G-1d and G-1e, specifically in the kinetics of HA-formation in the static-SBF tests (Fig. 3) as well as the kinetics and the induced HA-formation over monetite in the semi-dynamic SBF experiments (Figs. 4 and 6). These small differences in the mineralization behaviour are certainly related to the particular structural features of the two investigated glasses. Considering the similarities of the two glasses (suggested in Table 1 and reflected in the spectra of intact glasses in Figs. 3 and 6), a novel mathematic way

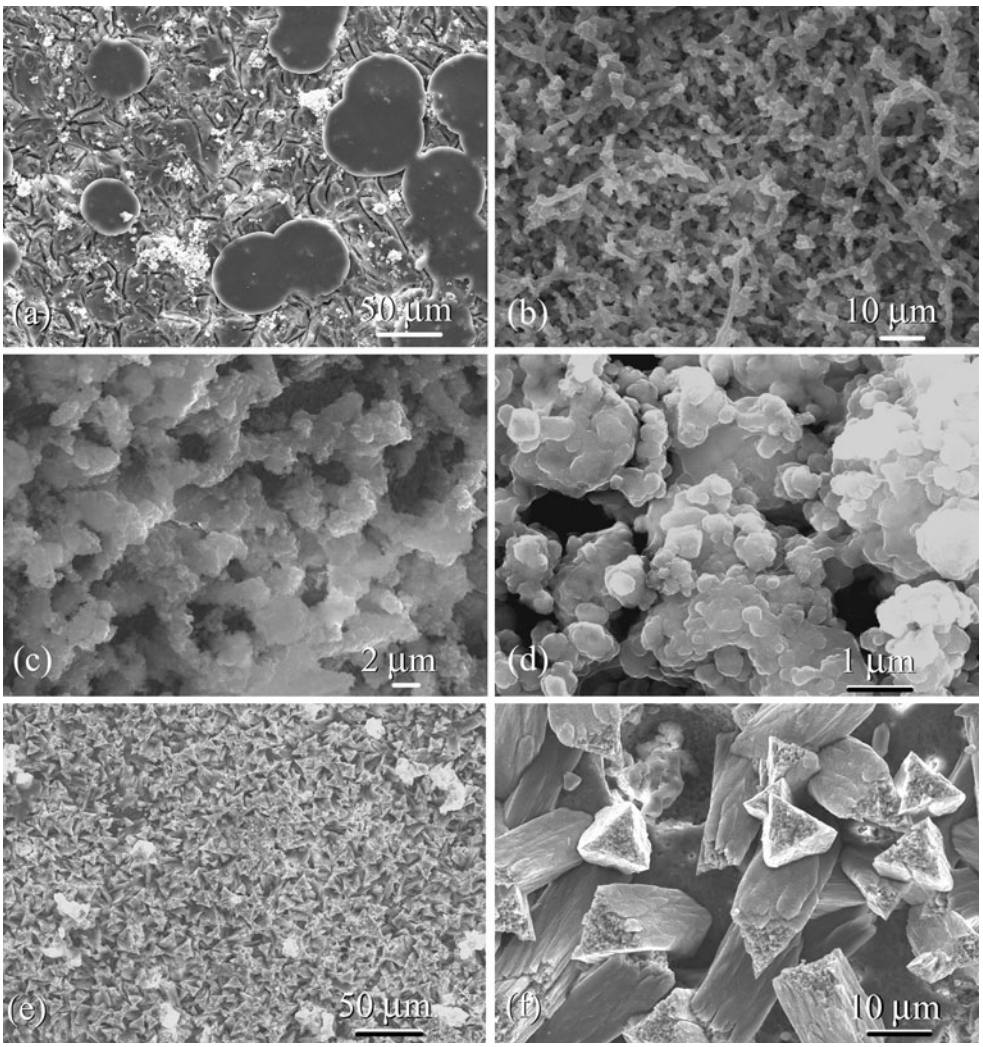

Fig. 5 Calcium phosphates developed on the surface of bulk glass samples after different immersion times in renewable SBF ("semi-dynamic" experiments) at 37°C. **a** Glass G-1d for 1 day, (**b–d**) glass G-1d for 21 days, (**e–f**) glass G-1e for 21 days

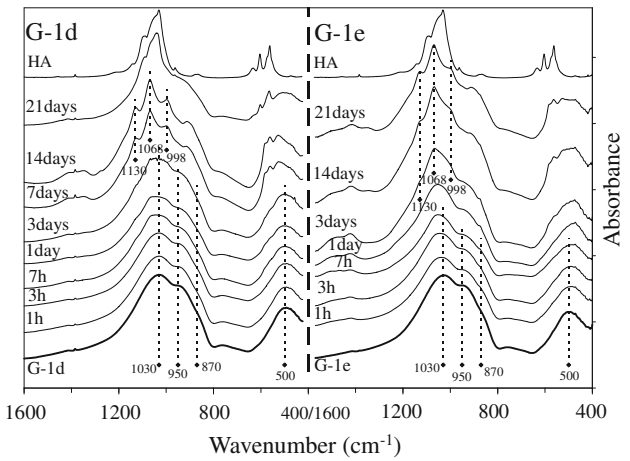

Fig. 6 Evolution of FT-IR spectra obtained from glass powders over immersion time in renewable SBF ("semi-dynamic" experiments) at 37°C. The spectrum of HA is also plotted for comparison purposes. (For facilitating comparison, the spectra have been normalized)

was developed to precisely determine the structural differences among them by subtracting their Raman spectra. According to this method, the difference between two spectra is calculated by minimizing the function $|RDS(v)|^2$, summed for all v (v = frequency) within the region where comparison has physical reason to be made. To subtract the spectrum of glass G-1d by the spectrum of glass G-1e, this function is $RDS_{de}(v) = D(v) - [C_1E(v) + C_2 + C_3v]$, where $D(v)$ is the frequency function of the glass G-1d and $E(v)$ that of glass G-1e. The parameters C_1, C_2, C_3 have the physical meaning of scaling and creating a baseline for each spectrum. The resultant spectrum "(G-1d)-(G-1e)" is plotted in Fig. 8.

According to Table 3, the Raman and IR spectra of Figs. 3 and 6 suggest that the glasses G-1d and G-1e are typical silicate glasses, built up with silica-tetrahedra and similar phosphates units. Hence, the broad positive band of Fig. 8 around 1050 cm^{-1} indicates an increasing

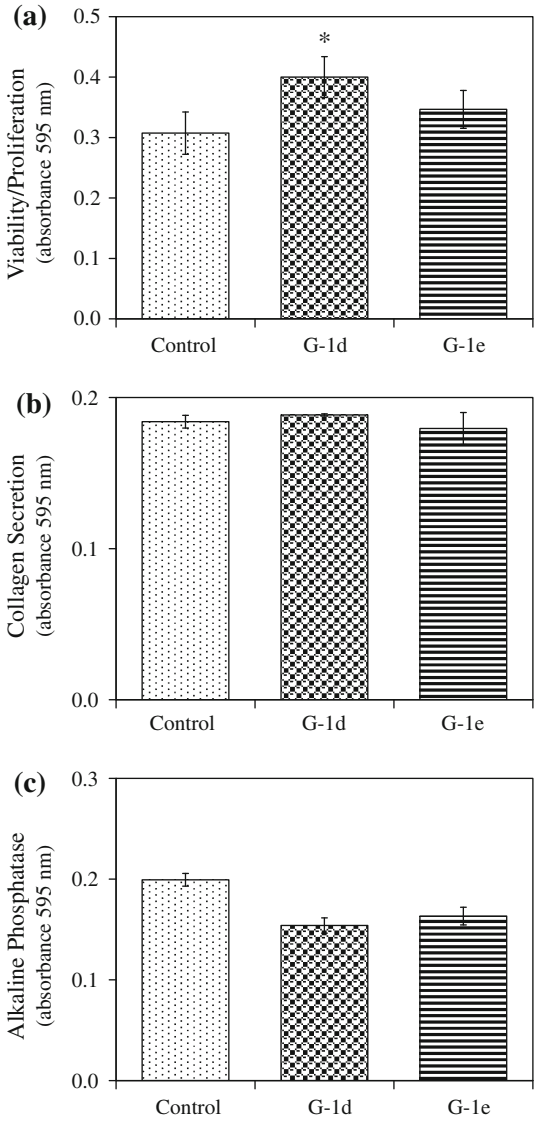

Fig. 7 1×10^5 osteoblasts were plated in the presence of glass powders G-1d and G-1e. After 72 h of incubation, viability/proliferation were evaluated by MTT assay (**a**), collagen production with SIRCOL assay (**b**), and alkaline phosphatase production by BCIP-NBT assay (**c**). Results represent mean values ± SD of duplicates from 8 (a), 4 (b), and 6 (c) different experiments ($P < 0.05$)

concentration of Si–O^0 bonds from bridging oxygens in Q^3, Q^2 and Q^1 structural units, which contain non-bridging oxygens (NBOs) in glass G-1d than in G-1e. The weak negative band between 790 and 980 cm^{-1} indicates a decrease in the formation of silicate units with bigger number of NBOs than Q^3, such as Q^2, Q^1 and Q^0. The difference in the distribution of silicate tetrahedral units in the network of these two glasses can be attributed to the slightly lower concentration of SiO_2 and higher concentration of Ca^{2+} ions ($\sim$2 mol% Table 1) in glass G-1e than G-1d. Hence, the silicate network of glass G-1e seems to exhibit a higher degree of depolymerization. It is well

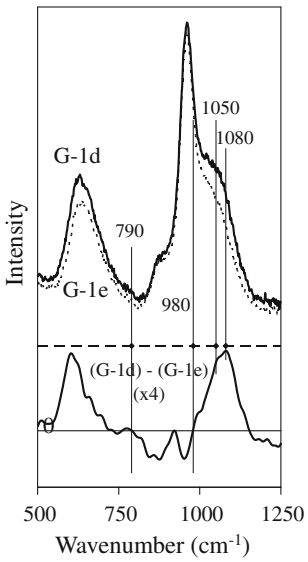

Fig. 8 Calculated spectrum "(G-1d)-(G-1e)" yielded by the mathematical subtraction of the Raman spectrum of intact glass G-1d by the relevant spectrum of glass G-1e, shown in Fig. 3. (The spectra of glasses G-1d and G-1e have been normalized. For better resolution, the spectrum "(G-1d)-(G-1e)" has been smoothened and multiplied 4 times)

known that smaller silicate units, such as Q^1 and Q^0, form when the concentration of modifier cations increases and that of formers decreases. Furthermore, the divalent Ca^{2+} cations, which have larger field strength than monovalent Na^+, prefer smaller silicate units with higher negative charge for charge neutralization.

The above differences between the structural features of the glasses G-1e and G-1d resulted in the aforementioned differences of their bioactivity performance in SBF. In the particular case of static SBF-tests (Fig. 3), the faster bioactivity response of glass G-1e (than G-1d) might be assigned to the less covalent network and the larger number of NBOs units (Si–O^-) than that in glass G-1d, since both factors are of high relevance for the bioactivity mechanism of silicate glasses [11–17]. With regard to the role of Ca^{2+}, the higher concentration of phosphate units in glass G-1e might cause slowing of the mobility of Ca^{2+} towards glass surface because Ca^{2+} ions prefer to interact with NBOs of phosphate units than with silicate ones [39]. The kinetics of Ca^{2+}-leaching from the glass is important in the case of renewable SBF tests because monetite formation indicates lower Ca^{2+} supersaturation regime in comparison to the conditions favouring the formation of HA. Accordingly, the above hypothesis anticipates a faster kinetics for the local increasing of Ca^{2+} supersaturation onto the surface of glass G-1d in comparison to glass G-1e. This would explain the preferential formation of HA onto the surface of glass G-1d after 3 weeks in renewable SBF, whereas monetite remains stable on the surface of glass G-1e (Figs. 4 and 6).

4.2 In vitro biocompatibility

Statements on the biological effects of a biomaterial require the use of cell cultures adapted to the tissue concerned. In the case of degradable, resorbable, or biomaterials which generally undergo significant surface modifications, such as the glasses investigated in the present study, the degradation products of bioactive glasses can stimulate the production of growth factors, cell proliferation and activate the gene expression of osteoblasts [22]. The experiments in the present work were carried out according to the methodology described in literature for primary culture of osteoblasts [24]. The aim was to preliminarily examine the influence of the materials on cell biology following internationally accepted criteria [40]. The results of in vitro tests do not show any evidence of toxicity or other detrimental effects on the functionality of osteoblasic cells, in good agreement with results reported for similar materials [41–45]. These results qualify the investigated glasses for further studies that might include cellular attachment, the molecular mechanisms involved in cell behaviour in the presence of these materials, gene expression patterns, which are critical for tissue engineering. Such studies will be required before further consideration and experimentation in biomedicine.

The increased osteoblasts' viability in the presence of both glasses, with especial emphasis in the case of glass G-1d (Fig. 7a), when compared to the control, is in good agreement with the inducing role of silicon [24] (glass G-1d is richer in Si than G-1e). The higher abundance of glass modifier Na^+ cations in glass G-1d might also enhance the viability of osteoblasts. On the other hand, the higher content of CaO in glass G-1e may reduce the flexibility of Ca^{2+} bound to phosphate units and annul the positive effect of Na^+ cations.

Osteoblasts' differentiation starts with proliferation of preosteoblasts, which are cells with lower potential to secrete alkaline phosphatase comparing to mature osteoblasts [46]. Calvaria derived bone cells have high proportion of preosteoblasts [47]. The results of Fig. 7c suggest that the investigated glasses may cause a delay in preosteoblast differentiation, which is not a serious concern. The presence of the glass powders did not cause any difference in collagen secretion (Fig. 7b). This is consistent a delay in preosteoblast differentiation because collagen is an osteoblast marker of the very early stages of differentiation [46]. The results shown in Fig. 7b and Fig. 7c do not oppose the alkaline phosphatase secretion data reported in Fig. 7a.

4.3 Structure–properties relationship and effect of heat treatment temperature

The temperatures of T_s and T_g, and the CTE-values are of great technological importance, the formers being closely related with the viscosity of the glasses (i.e. higher T_g implies higher viscosity) and the CTE determines the possibility of developing stable interfaces with other conventional inorganic materials used in medicine. These thermal properties are directly related to the network connectivity of the glasses [48]. Accordingly, the higher T_g and T_s and the lower CTE of the investigated glasses G-1d and G-1e than the B-containing parent glass G-1b (Fig. 1, Table 2) can be attributed to the change of the B_2O_3/SiO_2 ratio in the glasses [49] due to the substitution of B in the network of the glass structure via the schemes $2B^{3+} \rightarrow 1.5Si^{4+}$ (glass G-1d) and $2B^{3+} \rightarrow Si^{4+} + 0.2P^{5+} + 0.5Ca^{2+}$ (glass G-1e).

The absence of B in the compositions G-1d and G-1e did not significantly affect sintering and devitrification behaviour, which was similar to analogous B-containing glasses [39], resulting in completely dense samples of white colour after heat treatment at 800 and 850°C. However, in the case of glass G-1b (and other B-containing compositions), heat treatment at 850°C caused development of visible bubbles underneath the surface of the samples and a general properties decay of the glass-ceramics [39]. The differences observed might be due to an expected increase of the activation energy for viscous flow (E_{vf}) as a result of increasing both SiO_2-content and network connectivity in the B-free glasses. The E_{vf} values for SiO_2 (1100–1400°C) and for B_2O_3 (26–1300°C) are 710, and 347–50 kJ/mol, respectively [50].

It is also worthy noting that glass-ceramics G-1d and G-1e have a simpler phase assemblage (diopside, wollastonite and fluorapatite) in comparison to B-containing glass-ceramic G-1b (diopside, wollastonite, akermanite and fluorapatite) [39].

The intrinsic ability of the glasses G-1d and G-1e to be fully sintered (while in powder-compact forms) at relatively low temperatures (≥700°C) before crystallization starts in conjunction with the formation of the bioactive crystalline phases of wollastonite and apatite [3, 13, 20, 26] have to be highly considered for both expanding in vitro tests and extend the experiments towards in vivo tests in the future.

5 Conclusions

The new B-free bioactive glass compositions (designated as G-1d and G-1e) designed in the $CaO–MgO–SiO_2–Na_2O–P_2O_5–CaF_2$ system are promising for biomedical applications. In static-SBF tests, HA forms from the early stages of immersion and completely covers the surface of the glasses after 3 weeks. In daily renewable SBF tests the deposition of HA competes with that of monetite ($CaHPO_4$), a biocompatible calcium phosphate precursor of HA due to a local decrease of Ca^{2+} supersaturation. The novel mathematical method developed in the present study for

subtracting the Raman spectra of the intact glasses G-1d and G-1e enabled to reveal the structural features that are probably behind the somewhat different mineralization kinetics of the investigated glasses. These features are related to the contents of glass formers (silicate and phosphate units) and modifiers (Ca^{2+} and Na^{+}). The preliminary in vitro experiments with osteoblasts' cell-cultures demonstrate that the investigated glasses are biocompatible and there is no evidence of toxicity.

Sintering and devitrification of the B-free G-1d and G-1e glasses resemble the behaviour of analogous B-containing glasses. Heat treatment at 800 and 850°C result in white and completely dense glass-ceramics of diopside, wollastonite and fluorapatite.

Acknowledgments A. Balamurugan is thankful to CICECO for the post-doc fellowship grant. The financial support by the Greek Secretariat of Science and Technology, in the framework of the Project ENTER 04EP26, is also acknowledged.

References

1. Hench LL. The discovery of bioactive glasses, science, faith and ethics. London, UK: Imperial College Press; 2001.
2. Hench LL. Bioceramics. J Am Ceram Soc. 1998;81:1705–28.
3. Kitsugi T, Yamamuro T, Nakamura T, Kokubo TJ. Bone-bonding behaviour of MgO–CaO–SiO_2–P_2O_5–CaF_2 glass (Mother glass of A/W glass-ceramics). J Biomed Mater Res. 1989;23:631–48.
4. Ohtsuki C, Kokubo T, Yamamuro T. Mechanism of apatite formation on CaO–SiO_2–P_2O_5 glasses in a simulated body fluid. J Non Cryst Solids. 1992;143:84–92.
5. Kim NM, Miyaji F, Kokubo T. Bioactivity of Na_2O–CaO–SiO_2 glasses. J Am Ceram Soc. 1995;78:2405–11.
6. Vallet-Regi M, Ragel CV, Salinas AJ. Glasses with medical applications. Eur J Inorg Chem. 2003;6:1029–42.
7. Queiroz CM, Agathopoulos S, Frade JR, Fernandes MHV. Network connectivity and bio-mineralization of $0.45SiO_2$–$(0.45-x)MgO$–xK_2O–$0.1(3CaO{\cdot}P_2O_5)$ glasses. Mater Sci Forum. 2004;455–456:383–7.
8. Skipper LJ, Sowrey FE, Pickup DM, Drake KO, Smith ME, Saravanapavan P, Hench LL, Newport RJ. The structure of a bioactive calcia–silica sol–gel glass. J Mater Chem. 2005;15:2369–74.
9. Karlsson KH. Bioactivity of glass and bioactive glasses for bone repair. Glass Technol. 2004;45:157–61.
10. Lefebvre L, Chevalier J, Gremillard L, Zenati R, Thollet G, Bernache-Assolant D, Govin A. Structural transformations of bioactive glass 45S5 with thermal treatments. Acta Mater. 2007;55(10):3305–13.
11. Kim CY, Clark AE, Hench LL. Early stages of calcium phosphate layer formation in bioglasses. J Non-Cryst Solids. 1989;113:195–202.
12. Kokubo T. Recent progress in glass-based materials for biomedical application. J Ceram Soc Jpn. 1991;99:965–73.
13. Kokubo T, Kushitani H, Ohtsuki C, Sakka S, Yamamuro T. Effects of ions dissolved from bioactive glass-ceramic on surface apatite formation. J Mater Sci Mater Med. 1993;4:1–4.
14. Cho SB, Miyaji F, Kokubo T, Nakanishi K, Soda N, Nakamura T. Apatite-forming ability of silicate ion dissolved from silica gel. J Biomed Mater Res. 1996;32:375–81.
15. Hill R. An alternative view of the degradation of bioglass. J Mater Sci Lett. 1996;15:1122–5.
16. Karlsson KH. Bioactivity of glass and its relation to glass structure. Glass Phys Chem. 1998;24:280–4.
17. Karlsson KH, Backman R, Hupa M. An equilibrium study of phosphate precipitation on bioactive glass. Key Eng Mater. 2002;218–220:103–8.
18. Wilson J, Yli-Urpo A, Happonen RP. Bioactive glasses: clinical application. In: Hench LL, Wilson J, editors. An introduction to bioceramics. Singapore: World Scientific; 1993.
19. Serra J, Gonzalez P, Liste S, Serra C, Chiussi S, Leon B, Perez-Amor P, Ylänen HO, Hupa M. FTIR and XPS studies of bioactive silica based glass. J Non Cryst Solids. 2003;332:20–7.
20. Yamamuro T. A/W glass-ceramic: clinical applications. In: Hench LL, Wilson J, editors. An introduction to bioceramics. Singapore: World Scientific; 1993.
21. Kokubo T, Kim HM, Kawashita M, Nakamura T. Novel ceramics for biomedical applications. J Aust Ceram Soc. 2000;36:37–46.
22. Yao A, Wang D, Huang W, Fu Q, Rahaman MN, Day DE. In vitro bioactive characteristics of borate-based glasses with controllable degradation behaviour. J Am Ceram Soc. 2007;90(1):303–6.
23. Wallace KE, Hill RG, Pembroke JT, Brown CJ, Hatton PV. Influence of sodium oxide content on bioactive glass properties. J Mater Sci Mater Med. 1999;10:697–701.
24. Valério P, Pereira MM, Goes AM, Leite MF. The effect of ionic products from bioactive glass dissolution on osteoblast proliferation and collagen production. Biomaterials. 2004;25:2941–8.
25. Agathopoulos S, Tulyaganov DU, Ventura JMG, Kannan S, Karakassides MA, Ferreira JMF. Formation of hydroxyapatite onto glasses of the CaO–MgO–SiO_2 system with B_2O_3, Na_2O, CaF_2 and P_2O_5 additives. Biomaterials. 2006;27(9):1832–40.
26. Kokubo T, Kushitani H, Sakka S, Kitsugi T, Yamamuro T. Solutions able to reproduce in vivo surface structure changes in bioactive glass-ceramics A-W. J Biomed Mater Res. 1990;24:721–34.
27. Silver IA, Deas J, Erecinska M. Interactions of bioactive glasses with osteoblasts in vitro. Biomaterials. 2001;22:175–85.
28. Amaral M, Costa MA, Lopes MA, Silva RF, Santos JD. Si_3N_4-bioglass composites stimulate the MG63 osteoblast-like cells. Biomaterials. 2002;23:4897–906.
29. Meleti Z, Shapiro IM, Adams CS. Inorganic phosphate induces apoptosis of osteoblastic-like cells in culture. Bone. 2000;27:359–66.
30. Medrado GCB, Machado CB, Valério P, Sanches MD, Goes AM. The effect of chitosan-gelatin matrix and dexamethasone on the behavior of rabbit mesenchimal stem cells. Biomed Mater. 2006;1:155–61.
31. Klein B, Bem-Bassat H, Solomon V. Structurally different bisphosphonates exert opposite effects in Alp. J Cell Biochem. 1998;68:186–94.
32. de Aza PN, Guitian F, Santos C, de Aza S, Cusco R, Artus L. Vibrational properties of calcium phosphate compounds. 2. Comparison between hydroxyapatite beta-tricalcium phosphate. Chem Mater. 1997;9:916–22.
33. Prado Da Silva MH, Lima JHC, Soares GA, Elias CN, de Andrade MC, Best SM, Gibson IR. Transformation of monetite to hydroxyapatite in bioactive coatings on titanium. Surf Coat Technol. 2001;137(2–3):270–6.
34. Xu J, Butler IS, Gilson DFR. FT-Raman and high-pressure infrared spectroscopic studies of dicalcium phosphate dihydrate ($CaHPO_4{\cdot}2H_2O$) and anhydrous dicalcium phosphate ($CaHPO_4$). Spectrochim Acta Part A. 1999;55:2801–9.
35. Siriphannon P, Kameshima Y, Yasumori A, Okada K, Hayashi S. Comparative study of the formation of hydroxyapatite in

simulated body fluid under static and flowing systems. J Biomed Mater Res. 2002;60(1):175–85.
36. de Aza AH, Velasquez P, Alemany MI, Pena P, De Aza PN. In situ bone-like apatite formation from Bioeutectic® ceramic in SBF dynamic flow. J Am Ceram Soc. 2007;90(4):1200–7.
37. Agathopoulos S, Tulyaganov DU, Marques PAAP, Ferro MC, Fernandes MHV, Correia RN. The fluorapatite-anorthite system in biomedicine. Biomaterials. 2003;24(7):1317–31.
38. Habibovic P, Gbureck U, Doillon CJ, Bassett DC, van Blitterswijk CA, Barralet JE. Osteoconduction and osteoinduction of low-temperature 3D printed bioceramic implants. Biomaterials. 2008;29:944–53.
39. Agathopoulos S, Tulyaganov DU, Ventura JM, Kannan S, Saranti A, Karakassides MA, Ferreira JMF. Structural analysis and devitrification of glasses based on the CaO–MgO–SiO_2 system with B_2O_3, Na_2O, CaF_2 and P_2O_5 additives. J Non Cryst Solids. 2006;352(4):322–8.
40. Hendrich C, Geyer M, Acheddin D, Schutze N, Eulert J, Thull R. A new osteoblast cell culture system for standardized testing of biomaterials. Biomed Tech. 1996;41:278–83.
41. Agathopoulos S, Tulyaganov DU, Valerio P, Ferreira JMF. A new model formulation of the SiO_2–Al_2O_3–B_2O_3–MgO–CaO–Na_2O–F glass-ceramics. Biomaterials. 2005;26:2255–64.
42. Hongo O, Mukainakano Y, Asano M, Kawanami M, Kato H. Clinical and histopathological observation of CaO–P_2O_5–MgO–SiO_2–CaF system glass ceramic tooth implants in monkeys. Nippon Shishubyo Gakkai Kaishi 1989;31(4):1119–29. (in Japanese).
43. Mukainakano Y, Hongo O, Asano M, Kawanami M, Kato H. Application of CaO–P_2O_5–MgO–SiO_2–CaF system glass ceramics to periodontal therapy. Histopathological observation after implantation in furcation bony defect in monkeys. Nippon Shishubyo Gakkai Kaishi 1989;31(4):1110–8. (in Japanese).
44. Tworzydło M, Laczka M, Rajwa B, Dobrucki J, Turyna B. Evaluation of biocompatibility of apatite-wollastonite ceramics in fibroblast cultures. Folia Histochem Cytobiol. 2000;38(3):133–41.
45. Ryu HS, Lee JK, Seo JH, Kim H, Hong KS, Kim DJ, Lee JH, Lee DH, Chang BS, Lee CK, Chung SS. Novel bioactive and biodegradable glass ceramics with high mechanical strength in the CaO–SiO_2–B_2O_3 system. J Biomed Mater Res A. 2004;68(1):79–89.
46. Hernandez Miguel MV. Analysis of the effects of glucocorticoides in cell proliferation and collagen synthesis via experimental studies with cell cultures of osteoblasts. Barcelona, Spain: Ph.D. Thesis of University of Barcelona; 2003 (in Catalonian Spanish).
47. Manda D, Grigorie D, Stefanovici G, Vladoiu S, Busu C, Galarasu R, Dumitrache C. Alkaline phosphatase—biochemical and histological marker for primary osteoblast in proliferative phase. Rom J Endocrinol. 2004;42(1–4):29–36.
48. Shelby JE. Introduction to glass science and technology. London: The Royal Society of Chemistry; 1997.
49. Sohn SB, Choi SY, Kim GH, Song HE, Kim GD. Stable sealing glass for planar solid oxide fuel cell. J Non-Cryst Solids. 2002;297(2–3):103–12.
50. Doremus RH. Glass science. 2nd ed. USA: Wiley; 1994. Chapter 6, pp. 103.